Image Stitching Technology for Police Drones Using an Improved Image Registration Method Incorporating ORB Algorithm

Yingzi Cong
School of Continuing Education, Criminal Investigation Police University of China, Shenyang 110854, China
E-mail: ccpcyz@163.com

Keywords: fusion ORB algorithm, image registration, police drones, drone imaging, image stitching

Received: March 8, 2024

Drone aerial photography technology can assist public security departments in conducting on-site investigations and evidence collection. The single-aerial image captured by drones has limited field of view. Due to the influence of reconnaissance scenes, there are various shooting angles and overlapping areas. An improved image registration algorithm was proposed based on ORB. This algorithm combined segmentation and denoising processing to evenly distribute ORB feature points throughout the entire drone image. On this basis, Laplace fusion algorithm was used to match the overlapping regions. The study compared the improvement of ORB with several other methods. Three sets of experiments were compared and analyzed with the other three different fusion algorithms. These experiments confirmed that the improved image registration method had significant improvements in accuracy and speed compared with existing methods. The improved ORB registration algorithm was superior to traditional ORB in registration accuracy and registration speed. This algorithm had a registration rate increase of 7.4% and a time reduction of 153.97 seconds. This method effectively improves the splicing effect. It also handles the details of the splicing seam well, providing a basis for police to analyze the scene.

Povzetek: Študija uporablja izboljšan algoritem registracije slik, ki vključuje ORB za tehnologijo združevanja slik pri policijskih dronih, izboljšuje natančnost in hitrost registracije ter zagotavlja boljše rezultate spajanja slik.

1 Introduction

The drone aerial photography system uses unmanned aerial vehicles, carrying image acquisition devices. Meanwhile, wireless transmission technology is utilized to quickly obtain low altitude high-resolution images [1]. With the development of science and technology, drones are widely used in various aspects of society, such as in industry. They can be used for safety monitoring in hazardous areas such as chemical sites and high-voltage lines [2]. Police drones are a new type of police equipment that has the advantages of convenience and efficiency in aerial reconnaissance. Meanwhile, police drones can provide key technical support for police [3]. Traditional investigation methods can no longer meet the growing demand for investigation and evidence collection. Because there are challenges such as road traffic congestion, uncertainty in the scope of investigation, and the increasing use of anti-investigation methods by criminals [4]. So in recent years, drones are well applied in areas such as counter-terrorism and stability maintenance, air defense surveillance, and target tracking [5-6]. Drone aerial photography technology can assist public security departments in on-site investigation and evidence collection, real-time command and dispatch. Drone aerial photography technology has important practical significance and broad application prospects in public security. Oriented Fast and Rotated Brief (ORB) is an algorithm used in image processing, mainly for feature detection and description. By combining FAST feature detectors and Brief descriptors, feature points in images can be quickly and accurately detected and described [7]. Compared to other feature detection and description algorithms, ORB has significant advantages in speed and is widely used in fields such as object detection, tracking, recognition, and stitching. At present, the data collected by police drones are limited to general video surveillance scenes. The construction of panoramic images is relatively scarce. For this purpose, the study intends to carry out research on drone aerial image stitching technology and apply it to evidence collection and investigation. This has significant practical significance for alleviating the current situation of insufficient police force in public security organs. Meanwhile, this paper can improve the efficiency of investigation and evidence collection.

The study consists of four parts. Firstly, a discussion and analysis of previous research are conducted. Secondly, an innovative drone image stitching technology is proposed in combination with ORB. Then, the proposed technology is tested and analyzed to verify its application value in police drones. Finally, a conclusion is drawn and future work prospects are presented.

ORB is an efficient, accurate, and widely used image

processing algorithm, which has a wide range of applications in the field of image registration. Image registration is also an important technical means in various image processing, which is also an excellent image processing technique.

Tian et al. proposed a novel similarity measure that combined cosine and other methods. It was combined with the directional features and ORB feature extraction of accelerated segmentation testing to achieve rapid image forgery detection. This image was segmented into overlapping image blocks, and each image block's feature points were extracted using ORB. Similarity and match text were calculated by similarity means. These two blocks having max similarity were identified. Combining these two methods could demonstrate good robustness to lighting and others [8]. Batista et al. used image analyzing means to extract features and established an animal thermal comfort model based on thermal image classification of 7/8 Holstein-Gil heifers. Using an ORB detector to extract features from thermal images could verify the differences in the image's pixel intensity. PCA indicated that Tcan, Tbac, Thea, and Tski had a better correlation in characterizing animal thermal comfort [9]. Wu et al. proposed a 3D measuring method using feature correspondence. Only a frame of sine wave stripe pattern needed to be projected onto the tested object. Image correcting means were used to correct pixel size. A camera was used to capture five frames of deformation patterns, and the corresponding modulation patterns were extracted. The modified algorithm could assess mismatches and achieve pixel matching well [10]. Lin et al. proposed a CapsNetORB framework to achieve distorted target recognition and suppress deformation effects in the final prediction. The previous encoded vectors for the latter, while the latter detected interval dimensions with unchanged spatial scales to bridge the correlation between the source standard image and the distorted image. Therefore, the source standard image's category with the topmost correspondence was the final result [11]. Ma et al. proposed an ORB using a modified Quadtree Oriented Fast and Rotated Brief (QTORB). A new calculating method was put forward to elevate the algorithm's ability in uniform areas. QTORB managed and optimized feature points to remove overly intensive and coinciding points. QTORB could elevate features' distributing uniformity better [12].

With the continuous development of technology, image stitching technology has been widely applied in various fields. For police drones, it also plays an important role. To achieve better image stitching results, many researchers have improved image registration algorithms, which can be widely applied in multiple fields. Tang et al. proposed a fast sonar image stitching method, which included denoising, feature extraction, initial matching, stitching, and optimization. Based on the Euclidean distance between initial matching points and the inclination angle of the connecting line, poorly matched feature point pairs were removed to avoid incorrect matching [13]. Laarousi et al. proposed a new method. A new method was used in this experiment to distinguish moving objects. A map was created, where even in homogeneous regions, each pixel had the one-of-a-kind value within its surrounding environment. This method combined the early calculated mapping to quickly and effectively find the optimal seam [14]. Combining aerial imaging and visual analysis in open-pit mines, Winkelmaier et al. provided a new method for monitoring tension cracks, which might happen on workbenches or capture platforms excavated based on computer-aided design models. The size, location, and evolution of tension cracks were commonly used to predict slope failure and ensure safe mining operations. Clear photos were utilized in this experiment to depict cracks. Controllable filters, ENet, and UNet deep learning models were used to depict tension cracks. ENet adopted a left one cross-validation means to generate the excellent curve [15]. Hahn proposed a hyperspectral snapshot imaging method based on intermediate image plane diffraction. In this intermediate image, the planar diffraction microstructure was used to deflect light to the aperture where spectral filtering was performed. This method was related to imaging spectroscopy with reduced spectral resolution. Compared with filter-based hyperspectral snapshot imaging, it avoided the manufacturing difficulties of mosaic filter arrays, but spatial and spectral resolutions became coupled. This led to the uncertainty product of spatial and spectral resolution [16]. Legleiter et al. evaluated this method's potential to enhance retrieval by utilizing field observations of water depth and helicopter footage of clear flowing rivers. These results indicated that the depth inferred from the average image was more exact than that of a single image. The regression R-2 between observed and predicted values increased. IBARI elevated image depth maps' texture, making the representation of waterway morphology smoother and more coherent [17]. The relevant literature research is shown in Table 1.

Table 1: Related literature research

Reference	Method	Result	Limitation	Critical evaluation
Tian et al. [8]	Cosine and Jaccard similarity measures are combined with ORB feature extraction	High robust feature matching	Large consumption of computing resources	Computing efficiency needs to be improved
Batista et al. [9]	Animal thermal comfort model is established by ORB detector and PCA	Effectively classify thermal images	Image quality-dependent	The generalization ability needs to be verified
Wu et al. [10]	On-line 3D measurement and improved motion statistical feature algorithm	Robust pixel matching	Environment and equipment sensitive	Practicality needs to be enhanced
Lin et al. [11]	The CapsNetORB framework suppresses deformation effects	Improve the accuracy of target recognition	High computational cost	Framework needs to be simplified
Ma et al. [12]	QTORB algorithm optimizes feature point extraction	The feature points are evenly distributed	Application scenarios need to be adjusted	Experimental verification needs to be increased
Tang et al. [13]	Fast sonar image stitching	Improve stitching quality	Feature point selection is sensitive	The automation needs to be increased
Laaroussi et al. [14]	Dynamic object detection is combined with A* algorithm	Improve detection accuracy	High algorithm complexity	Practical applications need to be simplified
Winkelmaier et al. [15]	Deep learning models monitor tension cracks	Excellent model performance	Training data are in high demand	Adaptability needs improvement
Hahn et al. [16]	New method of hyperspectral snapshot imaging	Avoid filter manufacturing difficulties	Image quality is affected	Resolution needs to be optimized
Legleiter and Kinzel [17]	Evaluate deep retrieval potential	Extrapolating depth is more accurate	Subject to water conditions	Environmental adaptability needs to be enhanced

In summary, it is of great significance to study the image stitching technology of improved image registration methods based on ORB in police drones. In the future, ORB can be further improved on the existing basis. Therefore, more efficient and accurate feature point extraction and matching methods can be explored to achieve higher quality image stitching results. Meanwhile, ORB can further expand the application fields of image stitching technology and explore its application value in other fields.

2 Image registration based on improved ORB

Image registration is an important technical means. The main goal of image registration is to establish a transformation model between two images with overlapping regions and convert them into the same coordinate system. On this basis, a new feature-based registration method is proposed. SIFT, SURF, ORB, BRISK, etc. are compared and the optimal algorithm is selected.

2.1 Analysis of multiple algorithms based on feature extraction in image registration

Common image features used for feature extraction include spots, corners, inflection points, contours, and edges. Speckles are generally areas that differ in color or grayscale from surrounding pixels. Corner points are often the intersection of a corner or a line of an object in an image. Therefore, the noise resistance of corner points is stronger than corner points [18-19]. In spot detection, there are two classic spot detection methods: SIFT and SURF, while corner spot detection methods such as ORB and BRISK. In SIFT, firstly, the scale space of the image is established and the extreme values of the image are extracted. Secondly, interpolation is utilized to locate the pixels in the image and eliminate false points. When constructing a scale space, it is achieved through scale transformation, represented by formula (1).

$$G(x,y,\sigma)=\frac{1}{2\pi\sigma^2}e^{-\frac{x^2+y^2}{2\sigma^2}} \quad (1)$$

In formula (1), a Laplace transform is applied to it,

represented by formula (2).

$$\nabla^2 g = \frac{\partial^2 g}{\partial^2 x} + \frac{\partial^2 g}{\partial^2 y} \tag{2}$$

The result obtained through Laplace transform is represented by formula (3).

$$\nabla^2_{norm} = \sigma^2 \left(\frac{\partial^2 g}{\partial^2 x} + \frac{\partial^2 g}{\partial^2 y} \right) = -\frac{1}{2\pi\sigma^2} \left(1 - \frac{x^2 + y^2}{\sigma^2} \right) e^{-\frac{x^2+y^2}{2\pi\sigma^2}} \tag{3}$$

The Gaussian difference scale space of the image is represented by formula (4).

$$D(x, y, \sigma) = G(x, y, k\sigma) * I(x, y) - G(x, y, \sigma) * I(x, y) \tag{4}$$

In formula (4), $I(x, y)$ is a two-dimensional image. σ is the scale coordinate, which determines the smoothness of the image A smaller σ indicates a clearer image, while a larger σ indicates a more blurry image. Each pixel in the middle two frames of each group is detected in the degree of freedom space. The adjacent pixels consist of 8 adjacent pixels in this image. There are 18 pixels in the adjacent image, meaning 26 pixels need to be detected. Figure 1 shows the process of detecting extreme points in the scale space.

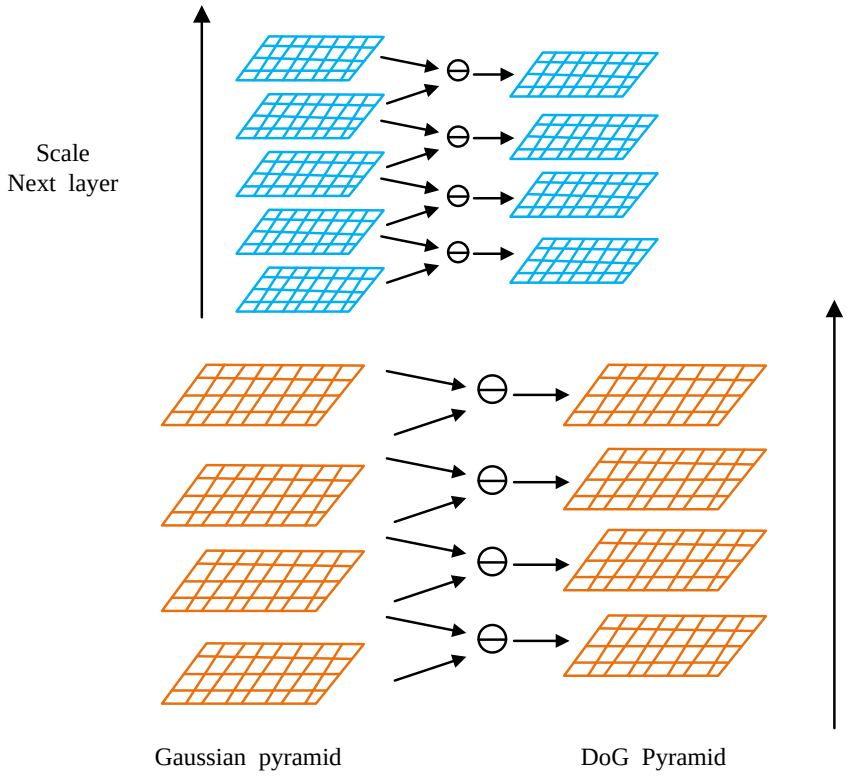

Figure 1: Scale space detection of extreme point process

From Figure 1, if this point is the maximum or minimum of 26 adjacent points, it can be considered as a feature point within this range. Extreme points are detected and pseudo points were removed in the scale space. The Gaussian difference scale space of the image is expanded using the Taylor formula, represented by formula (5).

$$D(X) = D + \frac{\partial D^T}{\partial X} + \frac{1}{2} X^T \frac{\partial^2 D}{\partial X^2} X \tag{5}$$

In formula (5), $\hat{X} = (x, y, \sigma)^T$ is the offset of the extreme value. The partial derivative of $D(X)$ is calculated and defined as 0. The position of the extreme point is represented by formula (6).

$$\hat{X} = -\frac{\partial^2 D^{-1}}{\partial X^2} \frac{\partial D}{\partial X} \tag{6}$$

From this, formula (7) can be obtained.

$$D(\hat{x}) = D + \frac{1}{2} \frac{\partial D^T}{\partial x} \hat{x} \tag{7}$$

If the deviation of the extreme point on any dimension exceeds 0.5, it is shifted along the offset direction until the offset between the sub-pixel points does not exceed 0.5. Then the point is considered a feature point. When $|D(\hat{x})| \le 0.03$, it indicates that the response value is relatively small and susceptible to noise. Meanwhile, this

pole should be removed. Firstly, the feature points are rotated, and then their neighborhoods are rotated to rotate in the direction of the feature points. Firstly, the 16*16 region where the feature points are located is segmented. Each sub-region is segmented to obtain the gradient values of each sub-region. This algorithm uses Gaussian weight function to calculate the weight of gradients in the neighborhood. The closer the algorithm is to the feature points, the greater its weight in Figure 2.

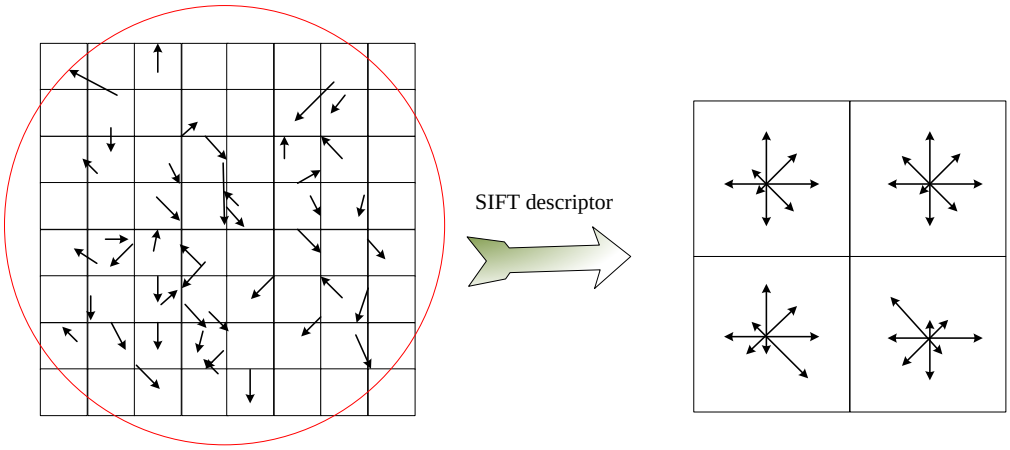

Figure 2: A schematic representation of the SIFT descriptor generation

In Figure 2, there are 16 sub-regions, each with 8 different gradients, totaling 16×8=128 values, forming a 128-dimensional SIFT descriptor. ORB applies the feature extraction method at FAST corners to feature extraction and optimizes this method. The FAST corner extraction method involves selecting 16 pixels from any pixel in an image on three discrete circles around it in Figure 3.

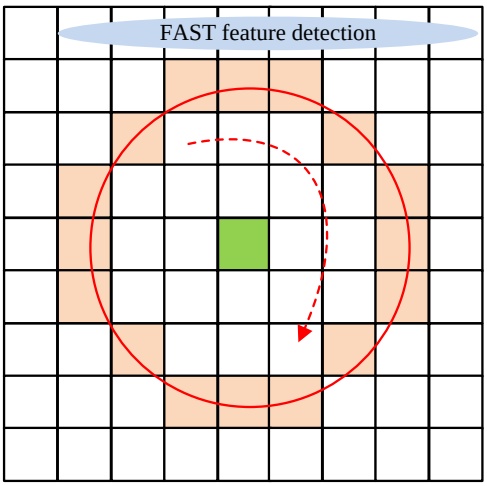

Figure 3: A schematic diagram of the FAST feature detection procedure

From Figure 3, if all n pixels out of the 16 pixels on the circle have pixel values larger than $I_p + t$ or smaller than $I_p - t$, then the point is considered as a corner point. I_p is the pixel value at the p point. t is a threshold. Usually, n takes 12 or 9. A grayscale histogram decomposition method based on wavelet transform is proposed. This method normalizes the grayscale histogram to obtain the grayscale histogram and normalizes the grayscale histogram. Firstly, FAST is utilized to sort the feature points in each layer of cone images. The Harris corner response values of feature points are calculated and sorted. The top N points are retained and expressed using formula (8).

$$\begin{aligned} R &= derM - \alpha(trM)^2 \\ M &= \sum_w \begin{bmatrix} I_x(x,y)^2, I_x(x,y)I_y(x,y) \\ I_x(x,y)I_y(x,y), I_y(x,y)^2 \end{bmatrix} \\ &= \begin{bmatrix} \sum_w I_x(x,y)^2, \sum_w I_x(x,y)I_y(x,y) \\ \sum_w I_x(x,y)I_y(x,y), \sum_w I_y(x,y)^2 \end{bmatrix} \end{aligned} \tag{8}$$

In formula (8), $I_x(x,y)$ and $I_x(x,y)$ are the partial derivatives of image $I(x,y)$. Based on the grayscale centroid of ORB, the orientation of feature points is obtained by utilizing the grayscale of pixels and the displacement of their adjacent centroids. The moment of one feature point's domain is represented by formula (9).

$$m_{pq} = \sum_{x,y} x^p y^q I(x,y) \tag{9}$$

The centroid of its corresponding neighborhood is represented by formula (10).

$$C = \left(\frac{m_{10}}{m_{00}}, \frac{m_{01}}{m_{00}} \right) \tag{10}$$

The angle between the feature point and the mass center is the principal direction of feature points, which is represented by formula (11).

$$\theta = a\tan 2(m_{01}, m_{10}) \tag{11}$$

The BRIEF descriptor is essentially a binary encoding that selects a set of point pairs centered on feature points and compares their grayscale values [20]. A binary comparison criterion function is defined for the neighborhood space and expressed using formula (12).

$$\tau(p;x,y) = \begin{Bmatrix} 1, p(x) < p(y) \\ 0, p(x) > p(y) \end{Bmatrix} \tag{12}$$

A binary string with a length of n can be obtained, represented by formula (13). This binary string is obtained by selecting multiple pairs of point sets around the feature points and comparing the judgment functions

$$f_n(p) + \sum_{1 \le i \le n} 2^{i-1} \tau(p; x_i, y_i) \tag{13}$$

ORB takes the main direction of feature points as the feature descriptor. Meanwhile, ORB adds a rotation matrix to its point-to-point matrix to ensure that the rotation of the descriptor remains unchanged. Firstly, n points near the feature points are combined to form a $2 \times n$ matrix, which is represented by formula (14).

$$S = \begin{pmatrix} x_1, x_2, ..., x_n \\ y_1, y_2, ..., y_n \end{pmatrix} \tag{14}$$

The rotation matrix corresponding to the direction of feature points is represented by formula (15).

$$R_\theta = \begin{bmatrix} \cos\theta, \sin\theta \\ -\sin\theta, \cos\theta \end{bmatrix} \tag{15}$$

The corresponding feature point pair matrix is represented by formula (16).

$$S_\theta = R_\theta S \tag{16}$$

The final feature descriptor after determining the direction is represented by formula (17).

$$g_n(p,\theta) = f_n(p) \big| (x_i, y_i) \in S_\theta \tag{17}$$

ORB uses a greedy search method to select the largest and smallest 256 pairs from all candidate point sets as feature descriptors. Therefore, the discriminability of BRIEF descriptors can be improved. An initial mask is first created for the image to be registered during mask construction and feature point positioning. The size of the mask is the same as that of the image, and the initial value is all zero. The improved ORB is used to locate the feature points on the initial mask. ORB quickly identifies the corner points in the image through the FAST corner detector. ORB is combined with the BRIEF descriptor for the feature description. An adaptive threshold is introduced in the algorithm to adjust the feature points extracted. Therefore, the distribution uniformity of feature points can be improved, and the uniform distribution of feature points can be ensured in the entire image range. After the feature points are located, the mask is updated to mark the positions of these feature points as 1 and keep the remaining positions as 0. In this way, the mask only retains the feature point information, which provides the basis for the subsequent image matching and fusion. When extracting feature points, the whole image is divided into several small blocks. Then the feature points are extracted independently in each small block. The minimum denoising algorithm is used to remove the clustered feature points and reduce the possibility of mismatching. The denoising process preserves scattered and distinguishable feature points by setting a threshold to identify. Meanwhile, those points that are too clustered are removed. For retained feature points, the ORB algorithm is used to generate descriptors.

2.2 Image stitching based on improved ORB in police drones

ORB only uses a fixed value to determine the required number of feature points. Therefore, ORB is not suitable for general situations and improves the speed and efficiency of matching. This project focuses on the characteristics of public security drone image acquisition and the problems existing in ORB. The uneven distribution of feature points in ORB is solved based on the method of image block segmentation. The clustering degree of feature points in ORB is improved through denoising methods. Figure 4 shows an optimized image matching method.

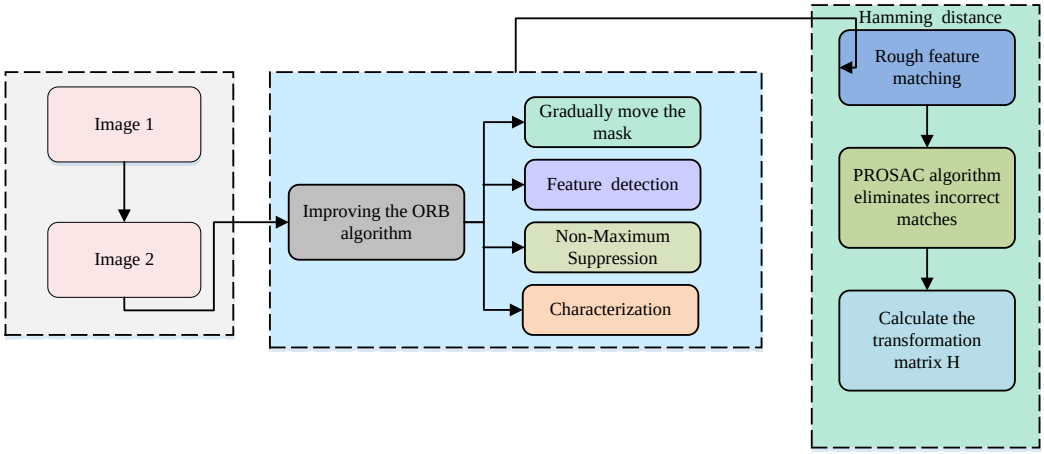

Figure 4: Process diagram for improving image registration methods

In Figure 4, first, the improved ORB algorithm is adopted for feature extraction in the registration of the two images. For the images to be registered, the study constructs a mask that will be used to identify and extract key feature points in the images. The construction of the mask is an iterative process. The feature points are accurately detected in different areas by gradually moving and covering the entire image. Then the ORB algorithm is used to locate the feature points at each mask position. The FAST corner detector and BRIEF descriptor are combined to detect and describe the feature points in the image quickly and accurately. A minimum denoising algorithm is used to identify and remove the clustered feature points by setting a threshold. Therefore, the quality of the feature points can be improved and the possibility of mismatching can be reduced. For retained feature points, the ORB algorithm generates descriptors that contain key information about the feature points, such as location, scale, and orientation. Then the whole image is traversed to obtain more feature points in a wider range and improve the accuracy of image registration. In the stage of feature point matching, hamming distance is used as the matching measure to measure the similarity between two feature descriptors. Meanwhile, the corresponding pair of feature points between two images can be found. The PROSAC algorithm is used to eliminate the wrong matching pairs and calculate the transformation matrix between images. The accuracy of matching is improved iteratively by adding matching pairs step by step and constructing a random sample consistency model. The Laplacian multi-resolution fusion algorithm is used for image fusion. When constructing the Laplacian pyramid, the top image and other levels do not use fusion rules, but directly use the original image data. The fusion process is shown in Figure 5.

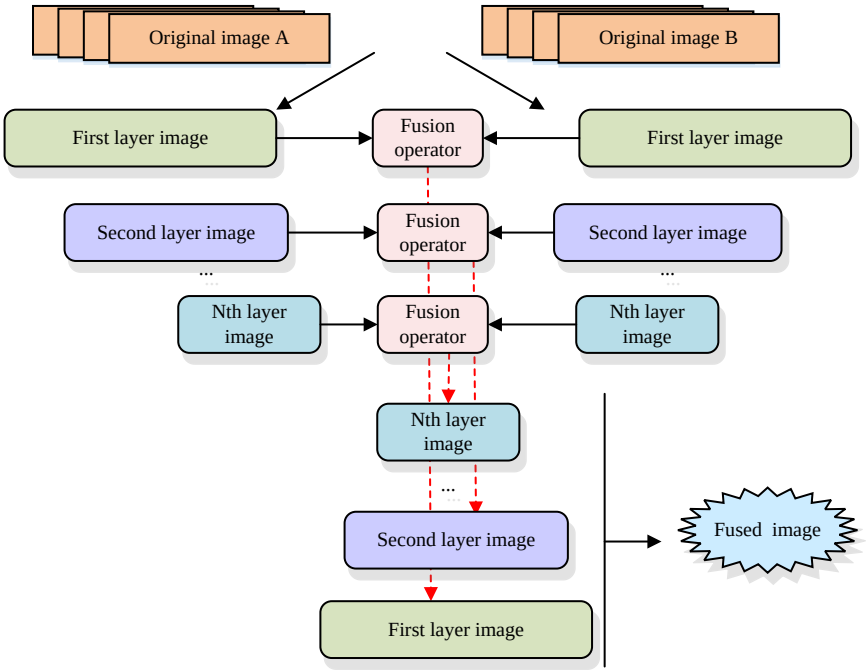

Figure 5: Multi-resolution fusion process based on Laplace

In Figure 5, the original images A and B are subjected to Laplace transform to obtain the first layer of images, respectively. The Nth layer of images is obtained sequentially by combing with the fusion operator. Pyramid reconstruction is performed on N-layer images to obtain fused images. In the improved image fusion algorithm, when establishing a panoramic view of the investigation area from police drone aerial images, it is necessary to ensure the clarity of the image and avoid "broken lines" and "ghosting". Traditional fusion methods cannot solve this problem well, but Laplace fusion can do this. Figure 6 shows an improved image fusion algorithm.

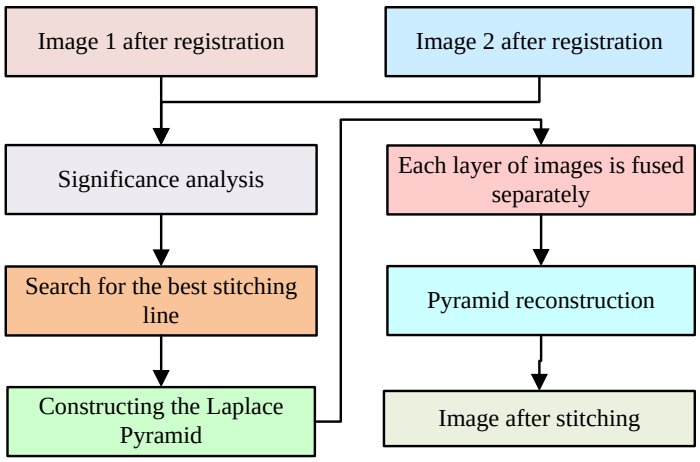

Figure 6: Improved image fusion algorithm flowchart

In Figure 6, the improved image fusion algorithm first performs image registration on these two images that need to be fused. Significant analyses are conducted on both. The optimal stitching line is searched by comparing the color and geometric differences between them. A Laplace pyramid is constructed to fuse images from each layer. The fused image is obtained after image stitching after pyramid reconstruction.

3 Comparative analysis of image registration and drone image stitching performance based on improved ORB

The study compared SIFT, SURF, ORB, and BRISK from multiple performance aspects through experiments to determine the optimal algorithm. This algorithm was optimized and improved, and its registration data were compared. Subsequently, the quality of the image obtained from stitching was evaluated.

3.1 Comparison of registration rates under different changing conditions among four registration algorithms

Four sets of image sequences with features such as scale and rotation, blur, perspective and lighting were selected. They were from the image library built in the Visual Geometry Laboratory at the University of Oxford. They were validated using 6 progressively increasing images as samples for the method. Four methods including SIFT, SURF, ORB, and BRISK were used to compare the feature matching rates and registration times. Faced with 6 images with scale, rotation, and blur changes, the first image was registered with the remaining 5 images based on SIFT, SURF, ORB, and BRISK in Figure 7.

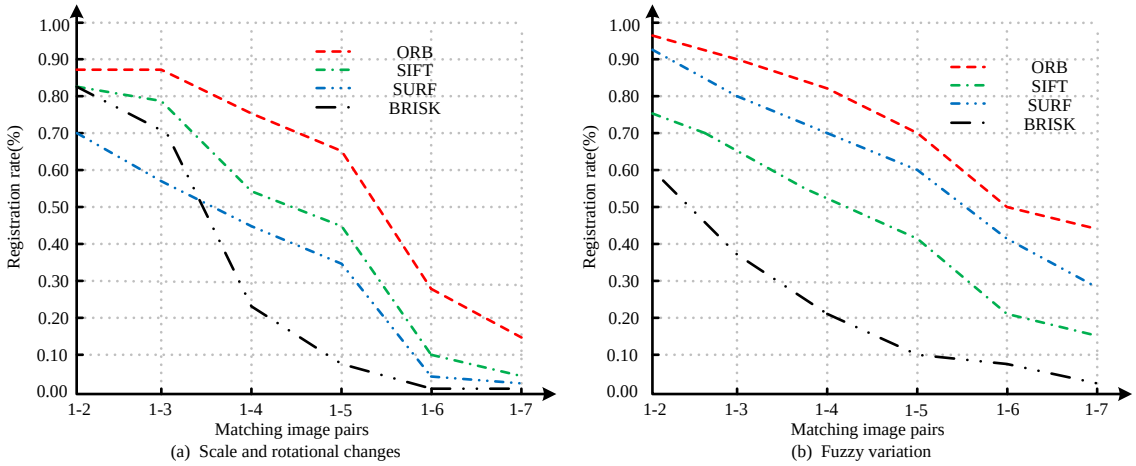

Figure 7: Comparison of registration rates of four algorithms under scale changes, rotation changes, and fuzzy changes

In Figure 7 (a), the accuracy of the SIFT, SURF, and ORB methods gradually decreased with increasing scale. The accuracy of BRISK decreased sharply within 1-4, and the robustness to scale and rotation was poor. In Figure 7 (b), the registration result of ORB was the best, followed by SURF and SIFT. The BRISK algorithm was the weakest. There were issues with changes in perspective and lighting in the image data captured by police drones. Therefore, four algorithms were used to register the images and obtain corresponding registration rates in Figure 8.

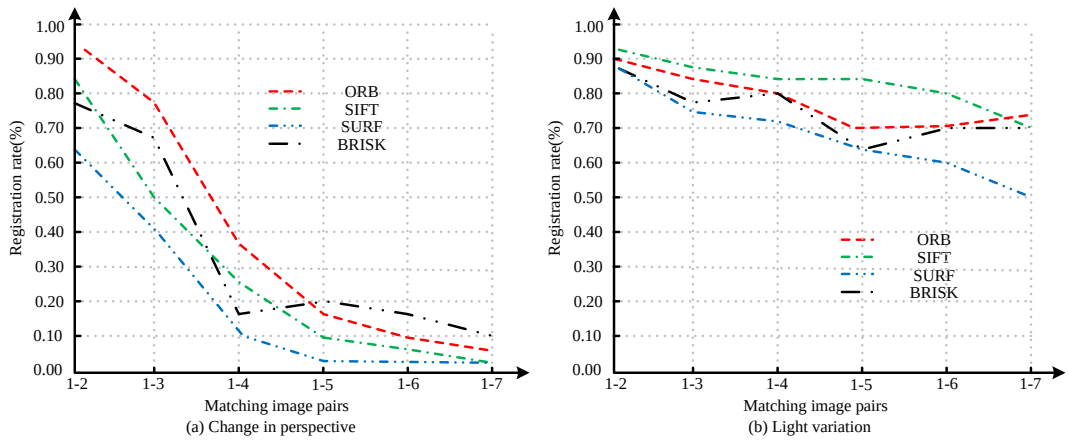

Figure 8: Comparison of registration rates of four algorithms under changes in perspective and lighting conditions

In Figure 8 (a), the registration results of the four methods were basically consistent. The registration performance of SIFT and ORB was slightly better. However, when there was a significant change in angle, the accuracy of all four methods decreased, resulting in weak robustness for large angle images. In Figure 8 (b), all four methods had good lighting adaptability, and there was a slight decrease in accuracy under different lighting conditions. The feature points, matching pairs, correct matching pairs, matching accuracy, and registration time of these two images under the influence of various objective factors were summarized in Table 2.

Table 2: Comparison of image feature point matching rate and matching time under objective changes

Change type/indicator	Algorithm type	Feature points in Figure 1	Feature points in Figure 2	Pairs	Correct matching	Matching accuracy	Matching accuracy standard deviation	Matching accuracy 95% confidence interval	Registration time(s)
Scale and rotational changes	SIFT	8679	8367	2567	2191	0.8535	0.020	[0.8335, 0.8735]	15.765
	SURF	3385	3405	1365	985	0.7216	0.015	[0.7011, 0.7421]	5.687
	ORB	502	502	275	243	0.8836	0.012	[0.8698, 0.8974]	0.962
	BRISK	2416	2424	312	265	0.8494	0.014	[0.8314, 0.8674]	2.105
Fuzzy variation	SIFT	3389	1803	756	539	0.7130	0.018	[0.6978, 0.7282]	15.355
	SURF	1446	986	724	615	0.8494	0.016	[0.8326, 0.8662]	5.757
	ORB	502	502	315	297	0.9429	0.013	[0.9291, 0.9566]	0.969
	BRISK	798	319	78	44	0.5641	0.022	[0.5458, 0.5824]	2.110
Change in perspective	SIFT	2486	3084	1065	865	0.8122	0.021	[0.7979, 0.8265]	15.769
	SURF	1093	765	505	321	0.6356	0.024	[0.6156, 0.6556]	5.705
	ORB	502	284	239	211	0.8828	0.020	[0.8682, 0.8974]	0.965
	BRISK	595	631	104	76	0.7308	0.023	[0.7146, 0.7470]	2.113
Light variation	SIFT	2436	2143	1136	996	0.8768	0.019	[0.8610, 0.8926]	15.739
	SURF	1533	1253	698	603	0.8639	0.017	[0.8499, 0.8789]	5.703
	ORB	502	502	240	214	0.8917	0.018	[0.8778, 0.9056]	0.967
	BRISK	873	687	203	166	0.8177	0.020	[0.8037, 0.8317]	2.113

In Table 2, under the type of scale rotation change, the ORB algorithm had the highest matching accuracy, reaching 0.8836 with a standard deviation of 0.012. The SURF algorithm had the lowest matching accuracy, 0.7216 with a standard deviation of 0.015. The registration time of the BRISK algorithm was the shortest, at 2.105 seconds. Under the fuzzy change type, the ORB algorithm had the highest matching accuracy, reaching 0.9429 with a standard deviation of 0.013. The BRISK algorithm had the lowest matching accuracy, 0.5641 with a standard deviation of 0.022. The registration time of SURF algorithm was the shortest, at 5.757 seconds. Under the type of perspective change, the SIFT algorithm had the highest matching accuracy, reaching 0.8122 with a standard deviation of 0.021. The SURF algorithm had the lowest matching accuracy, 0.6356 with a standard deviation of 0.024. The registration time of the BRISK algorithm was the shortest, at 2.113 seconds. Under different types of lighting changes, the SIFT algorithm had the highest matching accuracy, reaching 0.8768 with a standard deviation of 0.019. The SURF algorithm had the lowest matching accuracy, reaching 0.8639 with a standard deviation of 0.017. The registration time for ORB was the shortest, at 0.967 seconds. Overall, ORB showed high matching accuracy in most change types, while BRISK had the shortest registration time in most change types. When selecting a feature detection algorithm, it is necessary to choose a suitable algorithm based on specific application scenarios and requirements.

3.2 Application analysis of improved ORB fusion algorithm in drone image mosaic

The study selected two overlapping drone aerial images with a size of 3840*2160 to test the adaptability of this method to drone aerial images. By using SIFT, SURF, ORB, BRISK, and the proposed improved image registration method, these two images were registered and the registration results were verified. Figure 9 shows the registration rates and registration times for five different algorithms.

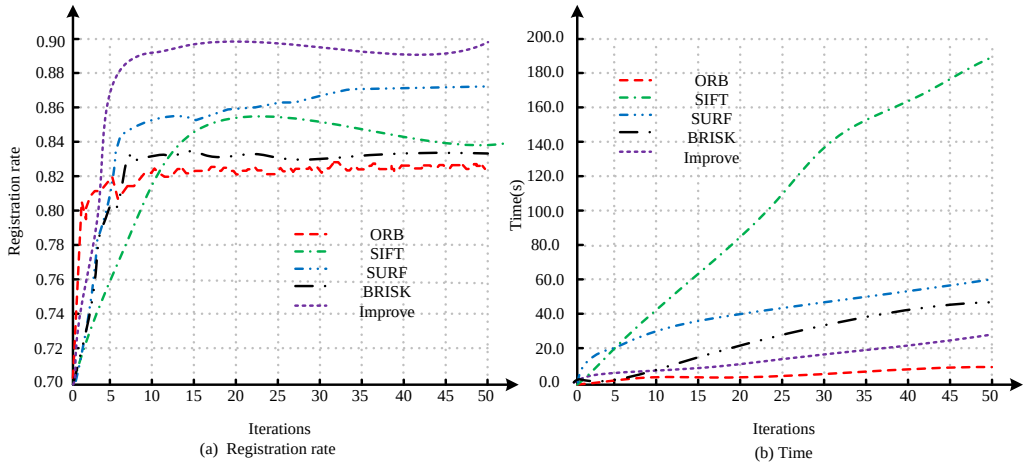

Figure 9: Registration data for ORB algorithm and improved algorithm

In Figure 9, this improved method was superior to the traditional ORB method in terms of registration accuracy and registration speed. The registration rate was increased from 82.89% to 90.29%. The standard deviation was 0.04%, an increase of 7.4%. The registration time is reduced from 189.33s to 35.36s. The standard deviation was 0.13s, which was reduced by 153.97s. Five different methods were used to extract features from drone aerial images. Preliminary feature matching was performed. On this basis, PROSAC purified specific matching pairs, removed incorrect pairs, and obtained the accuracy and time of registration for five algorithms.

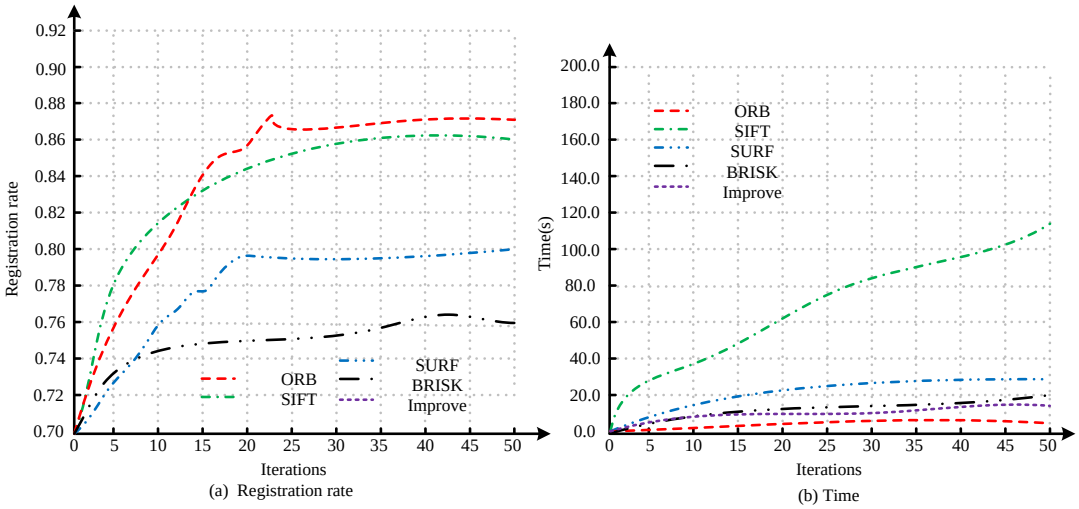

Figure 10: Registration data for ORB algorithm and improved algorithm

In Figure 10, this improved method had higher accuracy and higher registration efficiency than the traditional ORB method. The registration rate was increased from 87.89% to 93.49%. The standard deviation was 0.05%, an increase of 5.6%. The study tested the effectiveness of the improved fusion algorithm through three sets of experiments. Two images of 2300*1366 in size with translation and perspective changes were selected for experimentation. Firstly, an improved registration algorithm based on ORB was used for image registration. This algorithm was followed by direct averaging, gradual in and out, Laplace fusion algorithm, and improved fusion method for image fusion. For the evaluation of statistical features of a single image, commonly used objective evaluation indicators include information entropy, image mean and standard deviation, and average gradient. In this study, information entropy and average gradient were selected to evaluate the quality of concatenated images. Figure 11 shows the quality evaluation of the concatenated image obtained.

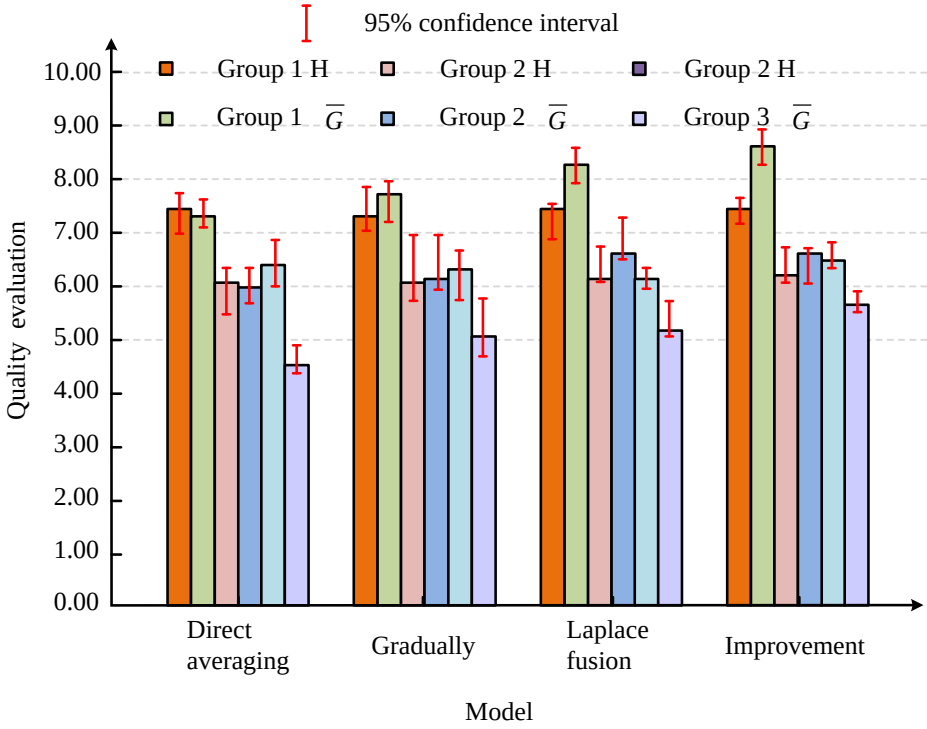

Figure 11: Quality evaluation of spliced images in three sets of experiments

In Figure 11, the improved algorithm resulted in improved stitching images in both information entropy and average gradient metrics compared with the other three methods. The improved algorithm improved the information entropy and average gradient of concatenated images. These images not only contained more information, but also had clearer details and textures. Especially in the third group of images with a large number of foreground targets, the significant improvement in average gradient further demonstrated. The improved algorithm had the advantage of preserving the details of the original image.

3.3 Discussion

The research method showed improved performance in multiple aspects compared with existing methods. Especially under the conditions of scale and rotation changes, the matching accuracy of the research method reached 0.8836. This method showed higher stability and accuracy compared to other algorithms. This improvement is mainly due to the denoising mechanism and Hamming distance matching strategy introduced in feature point detection and matching. This way effectively reduced the occurrence of mismatches. Under the condition of fuzzy changes, the performance of the research method was also outstanding, with a matching accuracy of up to 0.9429. The research method still maintained good registration performance even in dealing with degraded image quality. This is particularly important for image acquisition by drones in complex environments. Because the images captured by drones in practical applications are often subject to various interference. Compared with existing technologies, the research method had significantly improved in both information entropy and average gradient indicators. This result meant that the concatenated images not only contained more information, but also had clearer details and textures. Due to the optimization strategy in feature point extraction and image fusion stages, the research method effectively preserved the original details of the image while reducing visual distortion during the stitching. This algorithm-maintained efficiency and accuracy in multiple complex situations by introducing dynamic threshold adjustment and feature point quality evaluation mechanisms. This indicated that the research method had better environmental adaptability compared to existing methods.

4 Conclusion

Drone aerial photography technology can assist public security departments in conducting on-site investigations and evidence collection. Meanwhile, real-time command and dispatch can be conducted. The images captured by drones may be constrained by various factors such as shooting angle. Considering the characteristics of drone aerial images and the shortcomings of ORB, the detected feature points could be evenly distributed throughout the entire image based on the improved ORB registration algorithm. Through experimental verification, ORB was superior to other algorithms in terms of accuracy and registration speed. The improved ORB registration algorithm was also superior to traditional ORB in terms of registration accuracy and speed. The registration rate increased from 82.89% to 90.29%, an increase of 7.4%. The registration time decreased from 189.33 seconds to 35.36 seconds, a decrease of 153.97 seconds. The improved algorithm improved the information entropy and average gradient of the concatenated images. The details and textures of the images were also clearer. However, there are still shortcomings in the research. The current methods mainly optimize for specific drone models and environmental conditions. Different models of drones may have different camera specifications and flight characteristics. Different environmental conditions, such as lighting changes and weather conditions, may also affect image quality and registration results. Therefore, future work needs to consider the scalability of methods. Meanwhile, the study should explore how to adjust and optimize algorithms to adapt to different models of drones and diverse environmental conditions. In addition, extreme weather such as strong winds, rain and snow may affect the flight stability of drones, further affecting the quality of image acquisition. So further consideration is needed to combine and adapt with advanced flight control systems to enhance their applicability in various practical scenarios.

References

[1] E. D. Pusfitasari, J. Ruiz-Jimenez, I. Heiskanen, M. Jussila, K. Hartonen, and M. Riekkola, “Aerial drone furnished with miniaturized versatile air sampling systems for selective collection of nitrogen containing compounds in boreal forest,” Science of The Total Environment, vol. 808, no. 2, pp. 152011-152021, 2022. https://doi.org/10.1016/j.scitotenv.2021.152011

[2] C. Román, J. Llorens, A. Uribeetxebarria, R. Sanz, S. Planas, and J. Arno, “Spatially variable pesticide application in vineyards: Part II, field comparison of uniform and map-based variable dose treatments,” Biosystems Engineering, vol. 195, no. 7, pp. 42-53, 2020. https://doi.org/10.1016/j.biosystemseng.2020.04.013

[3] A. Georgiou, P. Masters, S. Johnson, and L. Feethan, “UAV-assisted real-time evidence detection in outdoor crime scene investigations,” Journal of forensic sciences. Vol. 67, no. 3, pp. 1221-1232, 2022. https://doi.org/10.1111/1556-4029.15009

[4] J. P. Kuehner, “Gravity-driven film flow inside an inclined corrugated pipe: An experimental investigation of corrugation shape and tip width,” Physics of Fluids, vol. 34, no. 12, pp. 122113-122132, 2022. https://doi.org/10.1063/5.0134555

[5] Z. Tuckey, “An integrated UAV photogrammetry-discrete element investigation of jointed Triassic sandstone near Sydney, Australia,” Engineering Geology, vol. 297, no. 2, pp. 106517-106532, 2022. https://doi.org/10.1016/j.enggeo.2022.106517

[6] F. Lodesani, M. C. Menziani, S. Urata, “Evidence of multiple crystallization pathways in lithium disilicate: a metadynamics investigation,” The journal of physical chemistry letters, vol. 14, no. 6, pp. 1411-1417, 2023. https://doi.org/10.1021/acs.jpclett.2c03563

[7] D. Pronoy, K. Sujit, P. Amalika, M. Abhisek, M. Golam, K. Chintak, K. Manoj, Q. Mohammed, and N. Uday, “Electric field guided fast and oriented assembly of mxene into scalable pristine hydrogels for customized energy storage and water evaporation applications,” Advanced Functional Materials, vol. 32, no. 47, pp. 2204622-2204635, 2022. https://doi.org/10.1002/adfm.202204622

[8] X. Tian, G. Zhou, and M. Xu, “Image copy-move forgery detection algorithm based on ORB and novel similarity metric,” IET Image Processing, vol. 14, no. 10, pp. 2092-2100, 2020. https://doi.org/10.1049/iet-ipr.2019.1145

[9] P. H. D. Batista, G. Almeida, and H. Pandorfi, “Thermal images to predict the thermal comfort index for Girolando heifers in the Brazilian semiarid region,” Livestock Science, vol. 251, no. 9, pp. 104667-104676, 2021. https://doi.org/10.1016/J.LIVSCI.2021.104667

[10] H. Wu, Y. Cao, H. An, Y. Li, H. Li, and C. Xu, “Fast and robust online three-dimensional measurement based on feature correspondence,” Optical Engineering, vol. 60, no. 7, pp. 74101-74117, 2021. https://doi.org/10.1117/1.oe.60.7.074101

[11] Z. Lin, W. Gao, J. Jia, and F. Huang, “CapsNet meets ORB: A deformation-tolerant baseline for recognizing distorted targets,” International Journal of Intelligent Systems, vol. 37, no. 6, pp. 3255-3296, 2022. https://doi.org/10.1002/int.22677

[12] C. Ma, X. Hu, J. Xiao, and G. Zhang, “Homogenized ORB algorithm using dynamic threshold and improved quadtree,” Mathematical Problems in Engineering, vol. 2021, no. 1, pp. 6693627-6693645, 2021. https://doi.org/10.1155/2021/6693627

[13] Z. Tang, G. Ma, J. Lu, Z. Wang, B. Fu, and Y. Wang, “Sonar image mosaic based on a new feature matching method,” IET Image Processing, vol. 14, no. 10, pp. 2149-2155, 2020. https://doi.org/10.1049/iet-ipr.2019.0695

[14] S. Laaroussi, A. Baataoui, A. Halli, and K. Satori, “Dynamic mosaicking: combining A* algorithm with fractional Brownian motion for an optimal seamline detection,” IET Image Processing, vol. 14, no. 13, pp. 3169-3180, 2020. https://doi.org/10.1049/iet-ipr.2019.1619

[15] G. Winkelmaier, R. Battulwar, M. Khoshdeli, J. Valencia, J. Sattarvand, and B. Parvin, “Topographically guided UAV for identifying tension cracks using image-based analytics in open-pit mines,” IEEE Transactions on Industrial Electronics, vol. 68, no. 6, pp. 5415-5424, 2021. https://doi.org/10.1109/TIE.2020.2992011

[16] R. Hahn, F. E. Hmmerling, T. Haist, K. Michel, and W. Osten, “Detailed characterization of a mosaic based hyperspectral snapshot imager,” Optical Engineering, vol. 61, no. 1, pp. 15106-15115, 2020. https://doi.org/10.1117/1.OE.59.12.125102

[17] C. J. Legleiter, and P. J. Kinzel, “Improving remotely sensed river bathymetry by image‐averaging,” Water Resources Research, vol. 57, no. 3, pp. 51-76, 2021. https://doi.org/10.1029/2020WR028795

[18] N. Thakur, N. U. Khan, and S. D. Sharma, "A Two-Phase Ultrasound Image De-Speckling Framework by Nonlocal Means on Anisotropic Diffused Image Data," Informatica, vol. 47, no. 2, 2023. https://doi.org/10.31449/inf.v47i2.4378

[19] D. Al-Karawi, S. Jassim, A. Sayasneh, C. Landolfo, D. Timmerman, T. Bourne, and S. Jassim, “An evaluation of the effectiveness of image-based texture features extracted from static b-mode ultrasound images in distinguishing between benign and malignant ovarian masses,” Ultrasonic Imaging, vol. 43, no. 3, pp. 124-138, 2021. https://doi.org/10.1177/0161734621998091

[20] T. Gherbi, A. Zeggari, Z. A. Seghir, and F. Hachouf, "Entropy-guided assessment of image retrieval systems: Advancing grouped precision as an evaluation measure for relevant retrievability," Informatica, vol. 47, no. 7, 2023. https://doi.org/10.31449/inf.v47i7.4661